Materials selection for thermal energy storage systems in parabolic trough collector solar facilities using high chloride content nitrate salts

F. Javier Ruiz-Cabañas[1,*], Cristina Prieto[1], Virginia Madina[2], A. Inés Fernández[3], Luisa F. Cabeza[4]

[1]Abengoa Research, C/ Energía Solar nº 1, Palmas Altas, 41014-Sevilla.

[2]Materials for Energy and Environment Unit. Tecnalia Research and Innovation, Mikeletegi Pasealekua, 2, 20009 San Sebastián, Spain

[3]Department of Materials Science & Physical Chemistry, Universitat de Barcelona, Martí i Franqués 1-11, 08028 Barcelona, Spain

[4]GREA Innovació Concurrent, Universitat de Lleida, Edifici CREA, Pere de Cabrera s/n, Lleida, Spain

* Corresponding author: F. Javier Ruiz-Cabañas

Abengoa Research, C/ Energía Solar nº 1, Palmas Altas, 41014-Sevilla

Phone: 0034954996570

Cell: 0034618125761

Email: fjavier.ruiz@abengoa.com

Abstract

The increasing role of concentrated solar power (CSP) within the renewable energy portfolio is attributed to the possibility of integrating thermal energy storage (TES) systems. Then, CSP technology has become one of the most interesting clean options to deliver dispatchable power on demand. Nowadays, commercial facilities use high quality solar salts (60%:40% $NaNO_3$ and KNO_3 by weight) as storage medium due to the attractive properties of this fluid to be applied under CSP operation conditions. Taking into account that CSP installations are designed with really large TES systems containing tens of thousands of tons, the use of lower quality nitrates salts would reduce the molten salts inventory cost and finally the investment cost of the CSP storage systems at commercial scale. The most important drawback of selecting low quality nitrates salts for high temperature CSP applications is the corrosion impact produced by impurities. Accordingly, chlorides have been identified in the state of the art as the impurity with higher effect over corrosion. This work is focused on A516 Gr70 carbon steel corrosion performance evaluation under high-chlorides content nitrates salts (1.2% and 3% by weight) at 400 ºC. In addition, the feasibility of using the proposed low purity mixtures with current CSP facilities materials selection is analyzed. Results reported within this study show the critical effect of chloride content over corrosion mechanism producing lack of adherence between base metal and oxides layers in addition to corrosion products delamination and internal cracking. Then, the use of A516 Gr70 carbon steel is rejected for a long term design under solar salts containing chlorides content in the range 1.2-3% by weight being necessary a higher corrosion resistant materials selection. An improved materials selection focused on higher corrosion resistance alloys is discussed.

Keywords: Corrosion, carbon steel, A516 Gr70, solar salts, chlorides, thermal energy storage (TES)

1. Introduction

Nowadays, low carbon economy policies are increasingly strict and demanding to change current trends in energy supply which are unsustainable from economic, environmental and social point of view. Accordingly, there is a worldwide pressing need for the development of advanced energy technologies in order to address the global challenges of clean energy, climate change and sustainable development [1,2]. Therefore, renewable energies become in crucial players within this new scenario being the concentrated solar power (CSP) one of the most interesting clean energy alternative [3,4]. The increasing role of CSP technology has been associated to the possibility of integrating large scale thermal energy storage (TES) systems to adapt electricity production to daily energy demand [5-8]. TES systems based on nitrate molten salts are currently available at commercial scale by using an inorganic mixture composed by 60% $NaNO_3$ and 40% KNO_3 by weight, the so-called solar salts. Solar salts meet requirements such as high thermal stability, high energy density, and low vapor pressure, among others, to be considered as appropriate thermal energy storage medium for CSP facilities [9-13].

One of the most important drawbacks inherent to solar salts is the corrosiveness associated to this fluid at high temperature. The molten nitrate salts in combination with the metallic components (storage tanks, piping, heat exchangers, valves, among others) of solar power plants constitute a corrosive system with the molten salt acting as an electrolyte. Although metal alloys corrosion mechanisms are well known in numerous aqueous electrolytes, lack of knowledge has been detected regarding corrosion mechanisms of metals under solar salts operation conditions in CSP plants. The use of inappropriate materials selection could result in the deterioration of the alloy properties compromising its validity for the final application for which they were designed. Corrosion mechanisms in molten salts are highly influenced by the oxygen ions present in the corrosive environment. Accordingly, pO^{2-} defines the oxide ion activity being a direct function of the metal corrosion in the medium. E-pO^{2-} diagrams are commonly used as an alternative to Pourbaix diagrams to analyze the performance of metals in contact with molten salts at high temperature [14]. Molten salts corrosion mechanism is driven by two main stages. Firstly, an alloy oxidation phenomenon is produced generating the corresponding oxides layers depending on the alloying elements of the metal and molten salts nature. Subsequently, molten salt produces a fluxing action over the protective oxide layers deteriorating it by dissolution. Therefore, the transference of oxidizing species through the metal and the metal ions into the molten salt is favored initiating accelerated attack [15].

Regarding nitrate salts corrosion, the corrosive effect is inherent to the nitrate-nitrite equilibrium of these fluids at a given temperature. Once reduction reaction from nitrate to nitrite is produced, the anionic oxidation of the alloy is carried out in the corrosive medium via the following reactions (iron is taken as an example):

$$NO_3^- \leftrightarrow NO_2^- + O^{2-} \quad \textbf{(1)}$$

$$Fe + O^{2-} \leftrightarrow FeO + 2e^- \quad \textbf{(2)}$$

$$3FeO + O^{2-} \leftrightarrow Fe_3O_4 + 2e^- \quad \textbf{(3)}$$

The aggressiveness of nitrate baths could be enhanced by the formation of peroxide and superoxide ions in the medium by the following chemistry [16-18]:

$$O^{2-} + NO_3^- \leftrightarrow NO_2^- + O_2^{2-} \quad \textbf{(4)}$$

$$O_2^{2-} + 2NO_3^- \leftrightarrow NO_2^- + O_2^- \quad \textbf{(5)}$$

Impurities associated to typical $NaNO_3$ and KNO_3 grades used in solar applications such as chlorides, sulfates, carbonates, and nitrites, among others, could enhance the aggressiveness of solar salts over metallic materials. Accordingly, nitrates salts used for CSP applications are high quality $NaNO_3$ and KNO_3 grades containing low amount of impurities which increase the final cost of the storage medium (Table 1). Current CSP plants installations are designed with huge TES systems with thousands of molten salts tons, being the Solana Generation Station the plant with the larger molten salt inventory at commercial scale (125,000 metric tons of solar salts) [19]. Then, molten salt inventory cost is a very important item in the overall TES cost of a CSP plan. TES energy cost are shown in Fig. 1 for a 50 MW oil parabolic trough collector (PTC) installation with storage capacity from 1 hour to 15 hours. Molten salts cost is in the range of 23% to 48% of the total energy cost depending on installed storage capacity [10]. Taking into account that achieving fully dispatchable CSP plants is the objective of this type of facilities, molten salts inventory is one of the most important parameter for TES costs reduction.

Table 1. Typical compositions of commercial $NaNO_3$ and KNO_3 for solar applications

Purity/Impurities	$NaNO_3$	KNO_3
Purity (%wt)	98 – 99.5	99.3 – 99.6
Chloride (%wt)	0.1 – 0.6	0.1 – 0.2
Sulfate (%wt)	0.10 – 0.50	0.05 – 0.5
Carbonate (%wt)	0.10	0.02 – 0.1
Nitrite (%wt)	0.02	0.02
Magnesium (%wt)	0.02 – 0.1	0.01 – 0.05

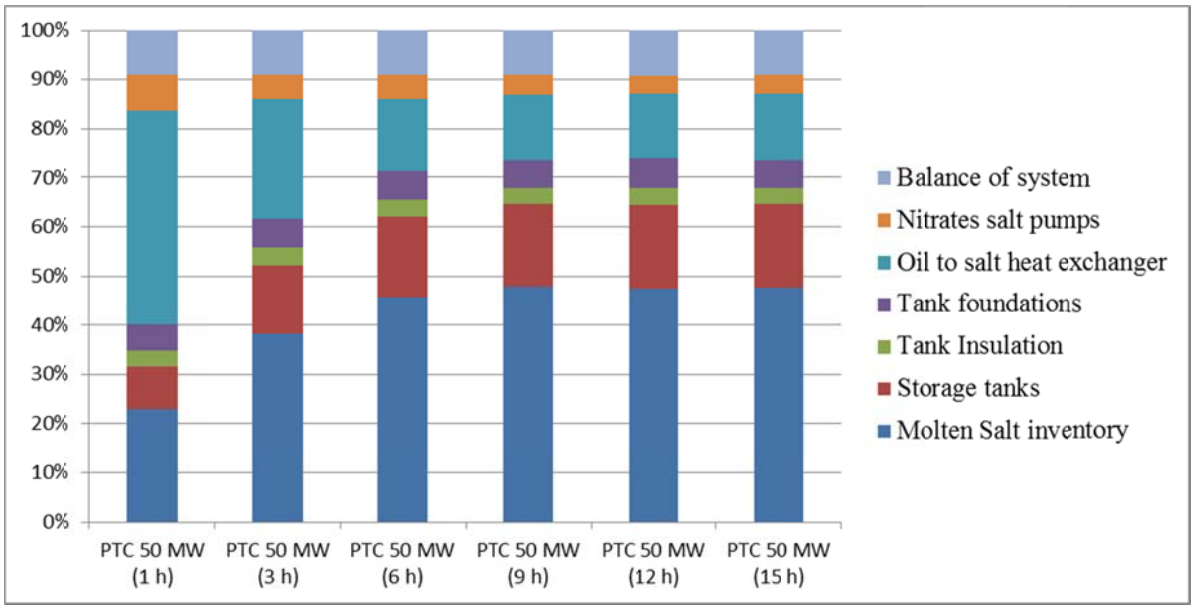

Fig. 1. Molten salts TES energy cost breakdown for 50 MW PTC plant with different storage capacities (1, 3, 6, 9, 12 and 15 hours). Adapted from [10]

Costs associated to current nitrate salts used in CSP TES systems are highly influenced by the final purity provided by the supplier. Then, the use of nitrate salts with higher impurity levels would reduce the cost of molten salts inventory and, therefore, the investment cost of the storage systems. The most important drawback of selecting low quality nitrates salts for high temperature CSP applications is the chloride content increasing (main impurity in industrial grades) which has been identified in the state of the art as the impurity with higher impact over corrosion. Chlorides increase molten salts aggressiveness over carbons steels and low alloyed steels due to the formation of chlorine (Cl_2) [20]. Once chlorine has been produced by de combination of chlorides ions, diffusion processes through oxides layer are produced. Chlorine reacts with the steel alloying elements to form metal chlorides at the steel/oxides layer interface (iron is taken as an example in chemical reactions (6) to (9)). Metal chlorides vapor pressure is relatively high at the interface and the evaporation of these species is produced (7). Then, metal chlorides diffuse back through the alloy oxides layers cracks and pores produced in the corrosion products of the steel. Finally, metal chlorides are oxidized to metal oxides as magnetite and hematite (8) and (9). Attending to chemical reactions (8) and (9), chlorine is again produced being this specie available to start the process described previously (chemical reactions (6) to (9)).

$$Fe + Cl_2 \rightarrow FeCl_2(s) \quad \textbf{(6)}$$

$$FeCl_2(s) \rightarrow FeCl_2(g) \quad \textbf{(7)}$$

$$3FeCl_2 + 2O_2 \rightarrow Fe_3O_4 + 3Cl_2 \quad \textbf{(8)}$$

$$2FeCl_2 + \frac{3}{2}O_2 \rightarrow Fe_2O_3 + 2Cl_2 \quad \textbf{(9)}$$

Several authors reported interesting results about the influence of chloride content in the corrosion performance of carbon steel showing a dependency between corrosion rates and chlorides content [21-24]. However, these results are associated to short corrosion tests which would be insufficient for a detailed evaluation of corrosion mechanism or longer thermal-corrosive treatments analyzing the effect of chloride content up to 1% by weight. Then, lack of knowledge has been detected about long term corrosion tests with nitrates salts containing chloride percentages higher than 1% by weight which would analyze the effect of low purity salts over metallic materials used in CSP facilities. Moreover, although the negative impact of chlorides over corrosion phenomena such as crevice corrosion and stress corrosion cracking (SCC) has been reported for different corrosive fluids [25-28], results associated to high chloride content nitrate salts have not been identified in the state of the art.

This paper is focused on the feasibility of using high-chlorides content nitrates salts as storage medium in PTC CSP installations. Then, corrosion performance of A516 Gr70 carbon steel under nitrates salts mixtures with different chlorides content levels was evaluated at 400 ºC (maximum design temperature of the storage system in PTC facilities). Experimental tests performed in this study complete previous results reported by the authors over carbon steel corrosion performance exposed to solar salts containing typical impurity levels for CSP application in the TES-PS10 pilot plant [29]. Summarizing, laboratory tests within this study face the following purposes: (i) To identify the corrosion mechanism induced by nitrate salts with high chlorides content by a sensitivity analysis with 1.2% and 3% by weight, over A516 Gr70 carbon steel; (ii) To quantify A516 Gr70 corrosion rates, analyze the performance of welded joints and evaluate SCC and crevice corrosion susceptibility; (iii) To compare results obtained in this study with carbon steel corrosion performance in the TES-PS10 pilot plant [29];

(iv) To discuss the feasibility of using solar salts with higher impurity levels at commercial scale with the current materials selection of parabolic trough collectors CSP plants; and, finally (v) To evaluate a higher corrosion resistant materials selection for this application.

2. Materials and methods

Thermal-corrosive treatment to evaluate the compatibility between A516 Gr70 carbon steel and high-chloride content nitrates salts was carried out using the so-called solar salts consisting in a binary nitrates mixture with a composition 60%:40% $NaNO_3$ and KNO_3 by weight close to the eutectic point (Fig. 2) [30]. Both nitrates salts, sodium and potassium nitrates, were supplied by SQM. Reagent grade NaCl was used to increase the chloride content adjusting it to 1.2% Cl^- and 3% Cl^- for Solar_Salt_1.2%Cl sample and Solar_Salt_3%Cl sample, respectively. Chloride determination was performed by Volhards´s method before and after NaCl addition to corroborate chloride concentration of the mixtures. Impurities associated to the final molten salts samples under evaluation are shown in Table 2.

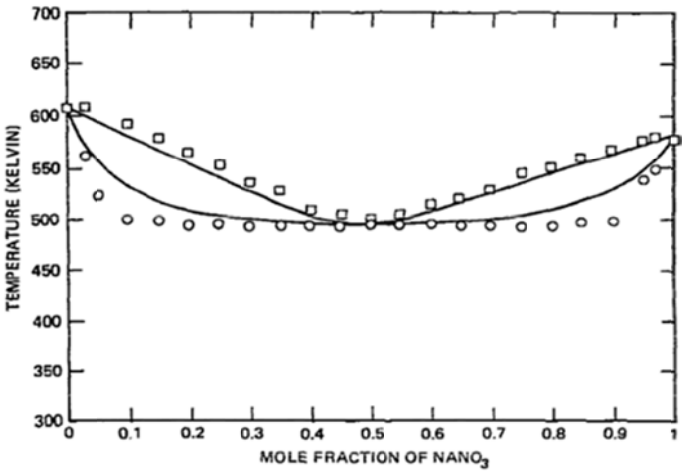

Fig. 2. $NaNO_3$-KNO_3 phase diagram [30]

Table 2. Molten salts samples impurities analyzed in the experimental tests

	Chloride (%wt)	Sulfate (%wt)	Carbonate (%wt)	Nitrite (%wt)	Magnesium (%wt)
Solar_Salt_1.2%Cl	1.2	0.34	0.1	0.02	0.068
Solar_Salt_3%Cl	3	0.34	0.1	0.02	0.068

The different corrosion coupons under study were assembled to metallic trees being placed inside the crucibles (Fig. 3). Corrosion coupons were electrically isolated using alumina washers to avoid any galvanic corrosion phenomenon between carbon steel specimens and the metallic tree as shown in Fig. 3. Each crucible was filled with one of the nitrate salt mixtures. The two crucibles containing the salt and the metal samples were introduced in a furnace. Corrosion tests were performed at 400 ºC under nitrogen atmosphere during 1581 hours, trying to simulate the most demanding conditions in parabolic trough collector CSP installations. Finally, corrosion coupons were extracted from the metallic crucibles once finished the corrosion test to evaluate the corrosion damage over A516 Gr70 specimens after nitrate salts exposure.

Fig. 3. Corrosion coupons assembly to metallic tree inside test crucibles before adding the salt

The metal alloy evaluated in this study was A516 Gr70 carbon steel, which is a structural alloy widely used in the manufacture of boilers, storage tanks and pressure vessel in many industrial sectors such as oil & gas and petrochemical for low and moderate working temperatures. Furthermore, this carbon steel is extensively used in CSP plants storage tanks where solar salts are used as storage fluid being the design temperature close to 400 ºC. The chemical composition associated to A516 Gr70 carbon steel is showed in Table 3 [31].

Table 3. Chemical composition of carbon steel A516 Gr70 [31]

Element	Percentage (%)
C	< 0.31
Si	0.15-0.40
Mn	0.85-1.25
P	< 0.035
S	< 0.035

An A516 Gr70 carbon steel plate was analyzed by optical microscopy (Motic BA210 trinocular compound microscope) before machining the different corrosion coupons to be exposed to the high temperature nitrates bath. Accordingly, metallographic specimens were manufactured by cutting metal sections from a carbon steel plate being embedded in resin and polished. A516 Gr70 showed a ferritic microstructure with pearlite bands as expected for this carbon steel. In addition, the microstructure grain size was between 9-10 according to ASTM-E112 (Fig. 4) [32]. Corrosion coupons were manufactured to analyze different corrosion damages such as uniform corrosion, stress corrosion cracking (SCC), and crevice corrosion, among others. All

corrosion specimens were cleaned before molten salts tests to assure that metal surface was completely free of dirt and metal splinters coming from machining processes.

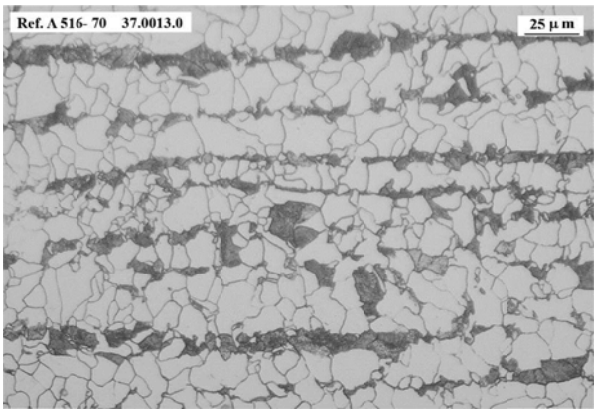

Fig. 4. A516 Gr70 microstructure before testing

Three rectangular parallelepiped coupons measuring 60 mm x 30 mm with a 10 mm diameter hole were machined to estimate carbon steel corrosion rates (two coupons without welding) and morphology attack characterization (one welded coupon) after 1581 hours under both nitrate salts corrosive treatments. Corrosion rates calculation was executed following guidelines extracted from ASTM G1-03 standard [33]. Oxides layers developed during the test were removed by applying a 50% HCl aqueous solution with the addition of 3.5 g hexamethylenetetramine (HMTA). This chemical solution eliminates the corrosion products generated by the steel, iron oxides mainly, without affecting the base material due to attack inhibition produced by the HMTA addition. The following equation (Eq. 1) was applied to obtain corrosion rates as µm/year [33]:

$$Vc = \frac{\Delta W}{S_0} \cdot \frac{K}{t \cdot \rho} \qquad \textbf{Eq. 1}$$

where, ΔW is the weight loss of the sample after testing and removing oxide layers (g), S_0 is the initial metallic surface in contact with the corrosive fluid (cm^2), K is a constant to express the final result as µm/year ($8.76x10^7$), t is the exposure time in hours, and ρ is the metallic alloy density as g/cm^3. Average corrosion rates were calculated by descaling two corrosion coupons. It was assumed that the total weight loss was only associated to uniform corrosion without taking into account localized phenomena which were evaluated by other methods within this work. In addition to corrosion rates calculation, corrosion damage penetration, oxides layer morphology, and localized phenomena such as intergranular corrosion (IGC), pitting, microstructure sensitization, and selective leaching of alloying elements, among others, was characterized by analyzing the welded coupon tested in the corrosion tests. Metal active gas (MAG) welding was executed over this corrosion coupon to identify possible corrosion attack differences between the welded metal, the heat affected zone (HAZ) and the base metal (Fig. 5a). Accordingly, coupon surface and transversal sections were studied with optical microscopy and also by scanning electron microscopy (SEM) by using SEM-JEOL 5910-LV microscope. Moreover, energy dispersive spectroscopy (EDS) spectra were performed using a microanalyser (EDS-OXFORD INCAx-act) coupled to SEM to characterize alloying elements in the surface of the coupon and the alloying element evolution thorough oxide layers generated over metallic alloys. Finally, Raman spectroscopy (785 nm laser) was performed to identify the stoichiometry of the iron oxides produced during the tests by using an Invia Reflex Renishaw Raman spectrometer.

A516 Gr70 SCC susceptibility under tests conditions was evaluated by using three U-bend coupons which were manufactured following indications extracted from ASTM G30-97 and ASTM G58-85 standards [34, 35]. Carbon steel plate sections were bended at 180º maintaining

the material deformation throughout the corrosion test. Three additional welded U-bend coupons were also used in this study to maximize residual stresses in the metal alloy. These specimens were fabricated by welding two rectangular sheets. Once welded, specimens were bended with the welding located in the bending axis. These types of SCC coupons introduce in the material residual stresses coming from both bending and welding processes. SCC phenomena susceptibility was checked by visual inspection and microscopic evaluation to identify cracks generation in the bending area of the non-welded/welded U-bend coupons under study. In addition to SCC evaluation, crevice corrosion sensitivity was evaluated using alumina devices to create overlapping surfaces where crevice attack could appear due to the formation of differential aeration zones as indicated by ASTM G78-01 [36]. Thus, alumina crevice devices were assembled to the straight section of one SCC coupons under evaluation as showed in Fig. 5b. Corrosion crevice damage was analyzed by visual and SEM examination after nitrates exposure.

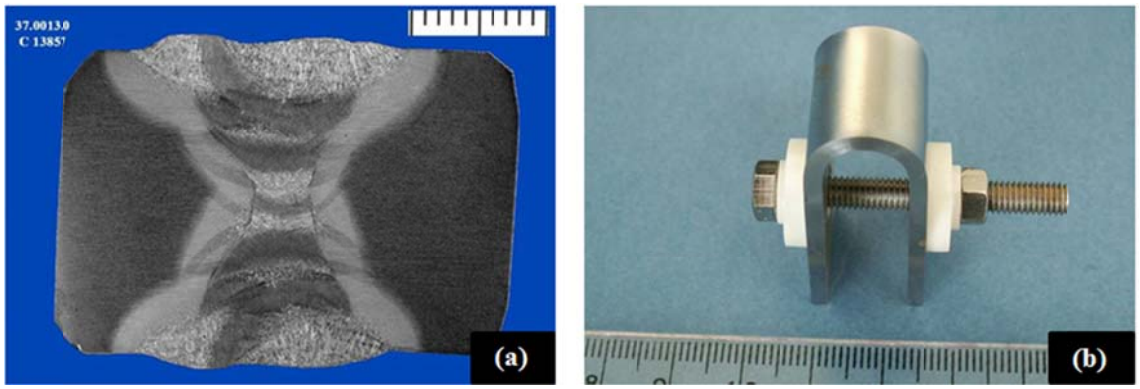

Fig. 5. Corrosion coupons manufacturing: (a) A516 Gr70 welded coupon before testing, (b) A516 Gr70 U-bend coupon for SCC and crevice corrosion susceptibility evaluation

3. Experimental results

3.1. Visual inspection

Once corrosion test finished after 1581 hours, A516 Gr70 corrosion coupons were extracted from metallic crucibles where they had been exposed to salt samples under evaluation, Solar_salt_1.2%Cl and Solar_salt_3%Cl. Then, carbon steel specimens were introduced in an ultrasound bath filled with distilled water at room temperature to eliminate nitrate salts adhered to metal alloy surface. Finally, corrosion coupons were dried with alcohol to perform a preliminary visual inspection over them.

Corrosion coupons tested under both salts samples showed uniform corrosion with brown-blackish oxides layers generation over base metal. Corrosion products were easily spalled from the base metal, as shown in Fig. 6 and Fig. 7. Corrosion damage extension seemed higher for the coupons tested in the salt sample with 3% by weight chloride content. This observation was confirmed within this study after corrosion rates calculation and microscopic examination supporting the important effect of chloride content in the carbon steel corrosion mechanism. Carbon steel corrosion coupons deterioration observed after testing (Fig. 6 and Fig. 7) contrasts with carbon steel specimens tested in the TES-PS10 pilot plant facility under CSP grade solar salts (chloride content close to 0.4%). These specimens developed very thin and compact oxide layers not detecting detachment of the corrosion products [29].

On the other hand, SCC susceptibility was not detected over U-bend coupons after visual inspection or 40x magnification inspection within this study. Similarly, no pitting or crevice

corrosion sensitivity was detected for A516 Gr70 specimens after testing under both molten salts samples. However, taking into account the high amount of corrosion products generated over the metal surface, pitting, SCC, and crevice corrosion susceptibility was analyzed more in detail once oxide layers were removed from the corrosion coupons. Finally, significant tonality changes or metallic particles precipitation was not detected in the molten salt samples after testing (Fig. 8).

Fig. 6. A516 Gr70 coupons after testing in Solar_salt_1.2%Cl: (a) Metallic tree and corrosion coupons assembly, (b) rectangular parallelepiped coupons set, (c) non welded U-bend coupons, and (d) welded U-bend coupons

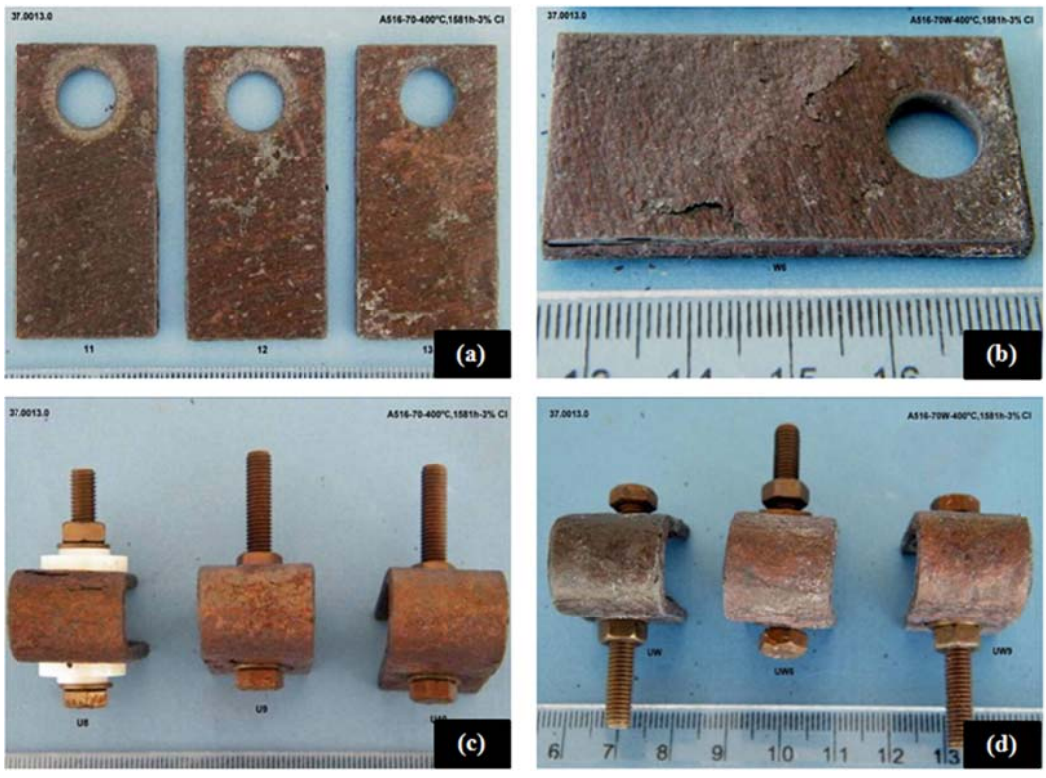

Fig. 7. A516 Gr70 coupons after testing in Solar_salt_3%Cl: (a) rectangular parallelepiped coupons set, (b) corrosion coupon detail, (c) non welded U-bend coupons, and (d) welded U-bend coupons

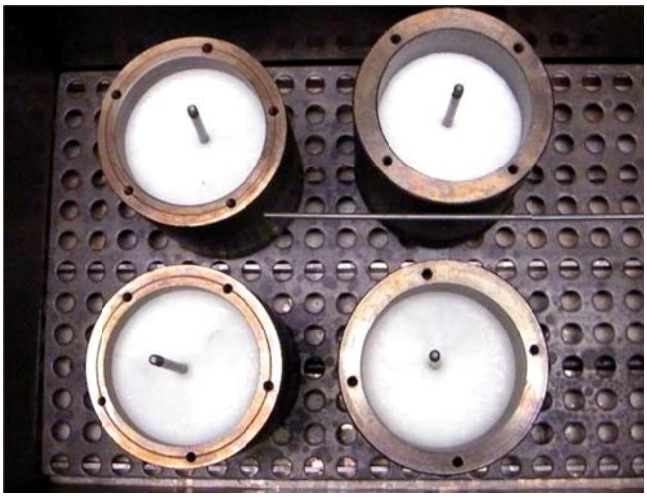

Fig. 8. Molten salts samples appearance after thermal-corrosive treatment

3.2. Microstructural characterization

Metallographic specimens were machined from the transversal metal section extracted from the base metal and welded areas of A516 Gr70 coupons tested in both nitrate mixtures. Once embedded in resin and polished, specimens were analyzed by optical microscopy to characterize the morphology and progression of corrosion damage through metal alloy. Optical micrograph displayed uniform corrosion over corrosion coupons not detecting localized phenomena such as pitting, intergranular corrosion, selective leaching of alloying elements, among others (Fig. 9). Oxides layers developed after corrosive treatments were not compact being detached from metal alloy under both molten salt samples under evaluation. Microscopic examination confirmed higher corrosion damage over metallic specimens exposed to the nitrates mixture with 3% by weight of chloride content. Accordingly, corrosion coupons developed thicker oxide layers with higher spalling phenomena after testing in Solar_salt_3%Cl sample (Fig. 9a and Fig. 9c). Consequently, oxides layers morphology suggested alloy passivation reduction with chloride content increasing compromising carbon steel resistance against nitrates corrosion. On the other hand, welded sections analysis showed higher corrosion damage penetration over the HAZ than observed in the base metal being this performance attributed to microstructural changes, phases precipitation and residual stresses induced by welding process in this area (Fig. 9b and Fig. 9d) [37, 38]. Morphology of the oxide layers produced with high chloride content was different from that developed by A516 Gr70 carbon steel exposed to low chloride content solar salts, which were completely adhered to the substrate producing the alloy passivation [29]. In conclusion, chloride ions play an important role in the corrosion mechanism of carbon steel degrading the adhesion of oxides layers to base metal and increasing porosity and delamination of corrosion products.

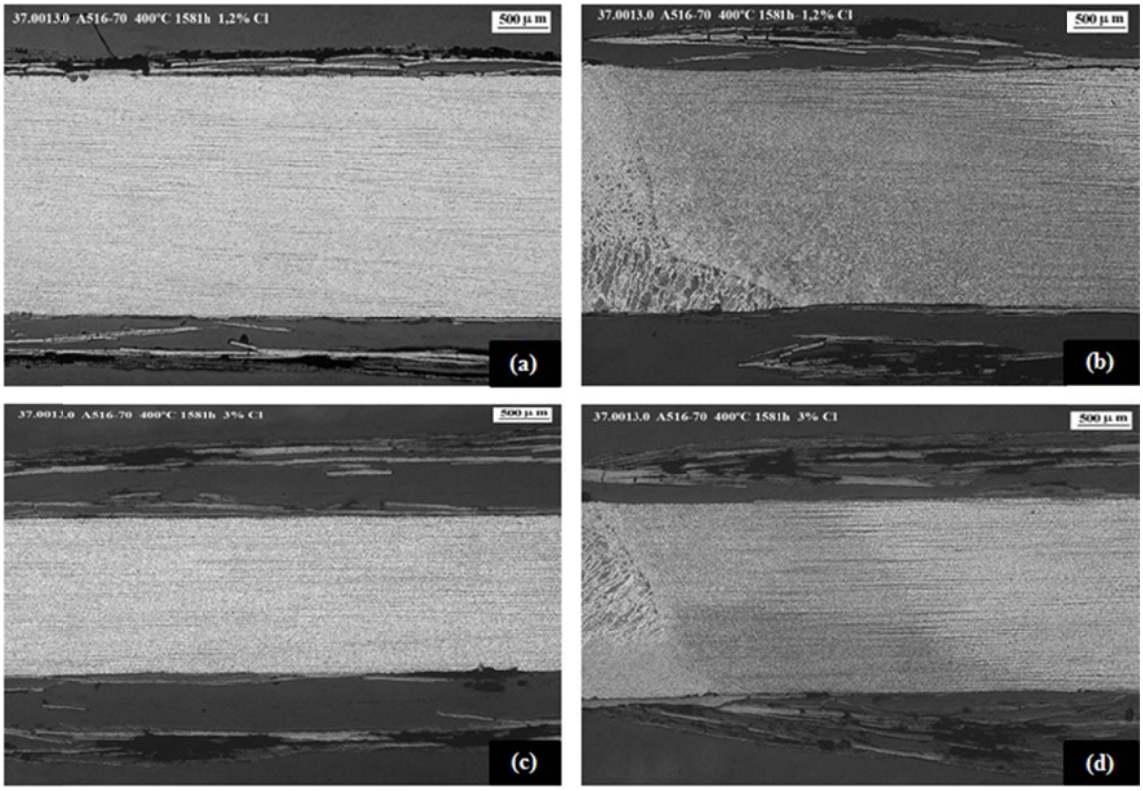

Fig. 9. A516 Gr70 microstructural characterization: (a) Non-welded corrosion coupon transversal section tested in Solar_Salt_1.2%Cl, (b) Welded corrosion coupon transversal section tested in Solar_Salt_1.2%Cl, (c) Non-welded corrosion coupon transversal section tested in Solar_Salt_3%Cl, and (d) Welded corrosion coupon transversal section tested in Solar_Salt_3%Cl

3.3. Corrosion products SEM/EDS and Raman analysis

Surface SEM/EDS analysis was performed over corrosion coupons exposed to both nitrate samples to characterize the morphology and chemistry of the corrosion products generated over the metallic specimens under evaluation. A516 Gr70 coupons did not show significant differences for both chloride concentrations developing oxide layers easily spalled and broken being this phenomenon particularly marked after Solar_Salt_3%Cl sample exposition. Therefore, corrosion products were not well adhered to the base metal indicating a lack of alloy passivation in addition to a non-protective performance, as shown in Fig. 10a for a corrosion coupon tested in Solar_salt_3%Cl sample. On the other hand, EDS spectra also showed similar chemical compositions for oxide layers generated by metallic coupons under both molten salt samples. Inner oxide layers were essentially composed by iron (Fe) and oxygen (O) being the iron oxide the main corrosion product generated during the test as expected (Fig. 10b). Additionally, the outer oxides layers showed a significant contamination with magnesium (Mg) which is a typical impurity in nitrate salts grades as showed in Table 1 and Table 2 (Fig. 10c). Finally, sodium (Na) and potassium (K) were also detected in the outer layers of corrosion products being these elements the main cations of the nitrate salts under evaluation (Fig. 10c).

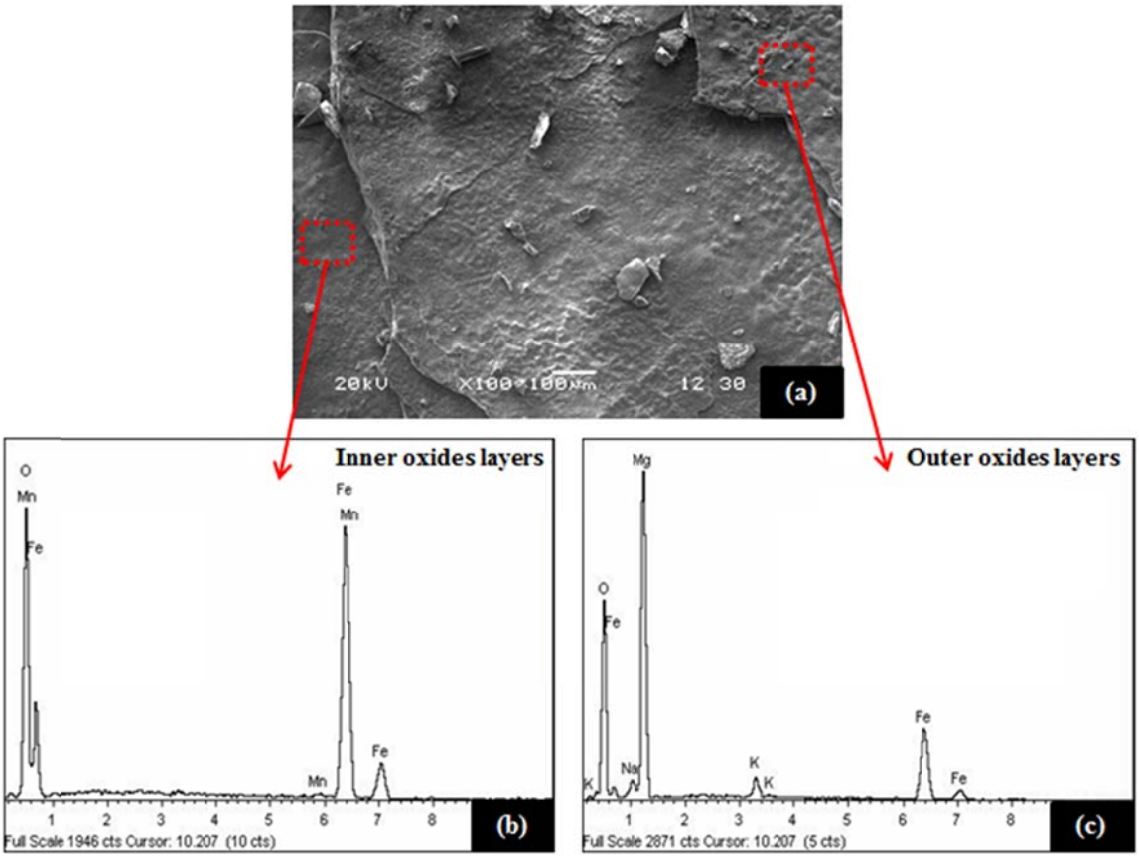

Fig. 10. Corrosion coupon surface SEM/EDS analysis: (a) Surface detail of coupon tested in Solar_Salt_3%Cl, (b) Inner oxides layers EDS spectrum, and (c) Outer oxides layers EDS spectrum

In addition to surface morphology analysis and associated chemical compositional evaluation, compositional scanning through A516 Gr70 corrosion coupons was performed by EDS mapping. Fig. 11 shows the electronic micrograph of the transversal section under evaluation (Fig. 11a) and associated element distribution profiles for Fe, O and Mg (Fig. 11 b-d). EDS mapping confirmed iron oxide as the main corrosion product developed during the test (Fig. 11b-c) and the deposition of Mg in the outermost layer (Fig. 11d). Finally, in order to characterize the iron oxides stoichiometry, Raman analysis were carried out over the transversal section of a metallographic specimen (Fig. 12). Raman spectra identified the iron oxides developed over the base metal as magnetite (Fe_3O_4) and hematite (Fe_2O_3). Results suggested that Fe_3O_4 was mainly located close to base metal (Fig. 12a) while Fe_2O_3 was in higher proportion in the outermost oxides layers (Fig. 12b) which is aligned with previous works. The formation of hematite and magnetite during the thermal-corrosive treatment is produced due to wustite (FeO) is stable only above 570 ºC. Previous electrochemical reactions, (2), (3), (8) and (9) and the following electrochemical reaction (10) are produced at 400 ºC [39]:

$$2Fe_3O_4 + O^{2-} \leftrightarrow 3Fe_2O_3 + 2e^- \quad \textbf{(10)}$$

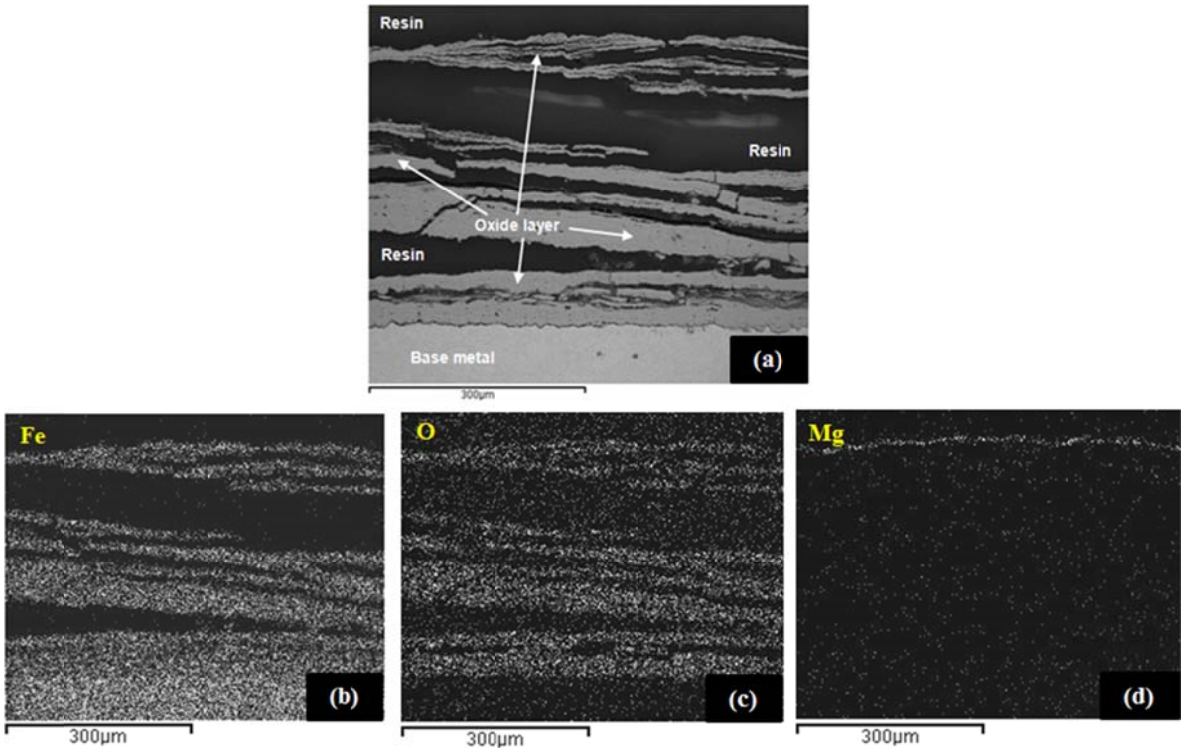

Fig. 11. Corrosion coupon EDS mapping: (a) Corrosion coupon transversal section SEM detail, (b) Fe distribution profile, (c) O distribution profile, and (d) Mg distribution profile

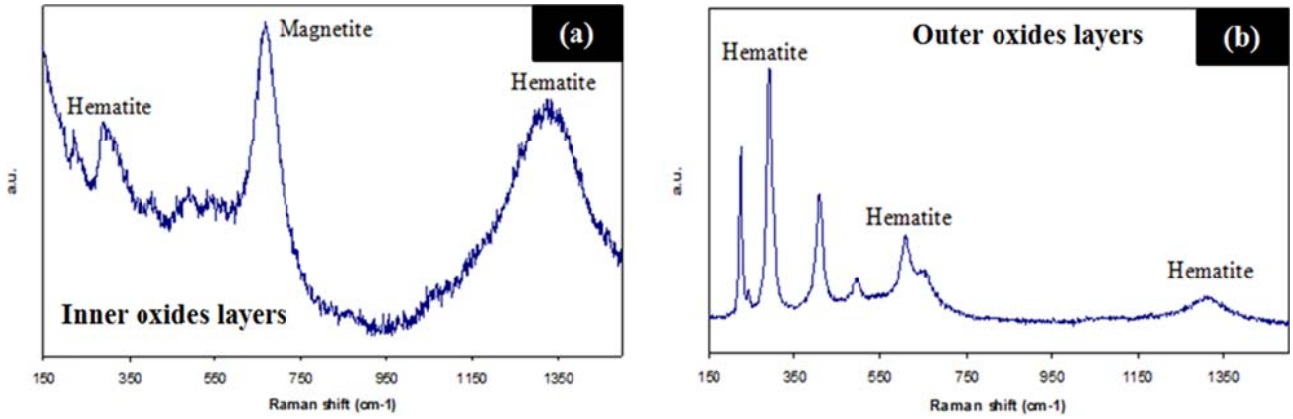

Fig. 12. Corrosion coupon Raman spectroscopy analysis: (a) Inner oxides layers Raman spectrum, and (b) Outer oxides layers Raman spectrum

3.4. Stress corrosion cracking and crevice corrosion sensitivity

Oxides layers generated over welded and non-welded U-bend coupons were removed to carry out a detailed evaluation focused on SCC and crevice corrosion damage (Fig. 13a). Then, metallic specimens were evaluated by magnifying glass (40x), optical microscopy and SEM. Cracks were not identified after visual inspection of the SCC coupons under both molten salts samples, Solar_salt_1.2%Cl and Solar_salt_3%Cl (Fig. 13b-c). Furthermore, U-bend specimen transversal sections were analyzed by optical microscopy not detecting cracks generation and propagation through metal alloy cross section for any coupon under evaluation (Fig. 13d). Accordingly, the combination of material, induced residual stresses, corrosive media, and operation condition evaluated within this test was not aggressive enough to produce catastrophic failures in the bending area of A516 Gr70 specimens. In addition to SCC damage, a crevice corrosion sensitivity was studied analyzing overlapped areas generated by the ceramic washers assembled in the U-bend coupons legs (Fig. 14a-b). Although detailed evaluation performed by

SEM displayed slight crevice corrosion damage in one of the coupon tested in Solar_salt_1.2%Cl (Fig. 14 c), A516 Gr70 crevice corrosion resistance was really high even for highly aggressive molten salt samples containing 3% by weight of chloride. In conclusion, A516 Gr70 carbon steel is found to be resistant to SCC and crevice corrosion phenomena after exposure to solar salts containing chloride levels up to 3% by weight at 400 ºC.

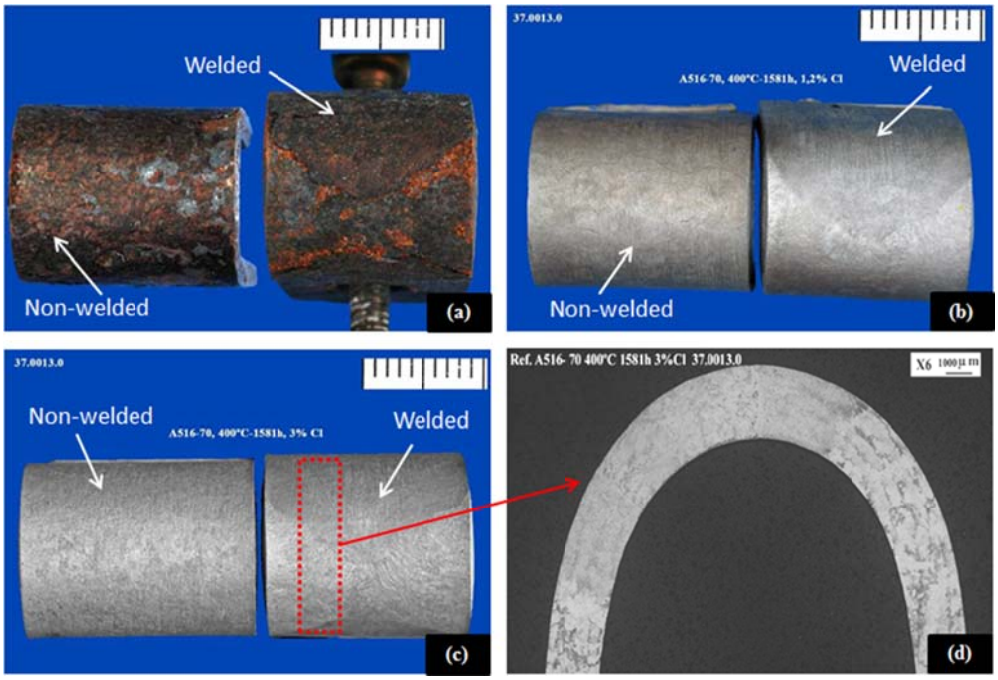

Fig. 13. SCC evaluation: (a) Welded and non-welded U-bend coupons after testing, (b) descaled U-bend coupons after exposure to Solar_salt_1.2%Cl, (c) Descaled U-bend coupons after exposure to Solar_salt_3%Cl, and (d) U-bend coupon transversal section microscopy

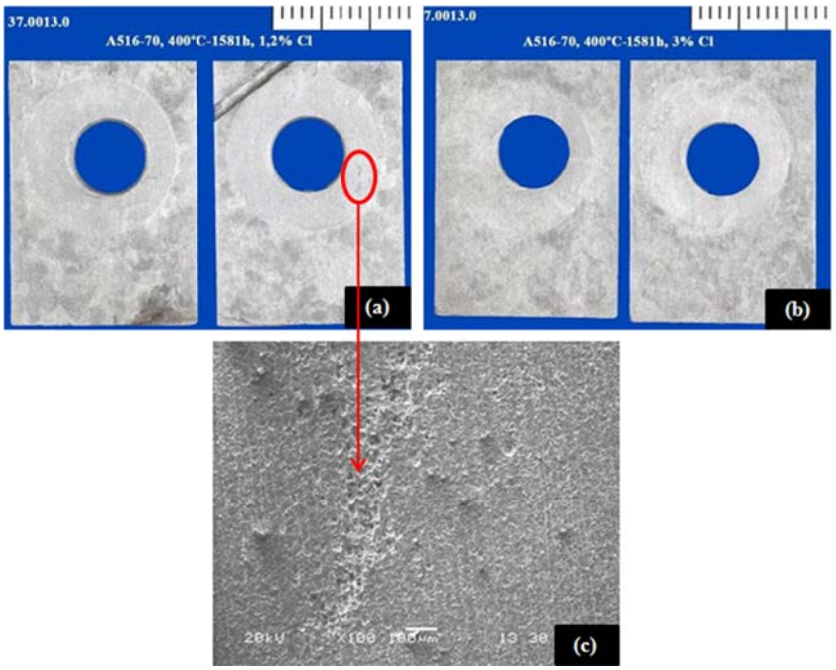

Fig. 14. Corrosion crevice evaluation: (a) descaled coupons after exposure to Solar_salt_1.2%Cl, (b) descaled coupons after exposure to Solar_salt_3%Cl, and (c) Crevice corrosion damage detail analyzed by SEM

3.5. Corrosion rates calculation

Corrosion damage indicators such as weight gain (mg/cm^2) and corrosion rates (µm/year) were calculated after thermal-corrosive testing to obtain quantitative data for the corrosion attack produced by both molten salts mixtures under study (Table 4). Therefore, two corrosion coupons were weighted before and after testing in the nitrates baths to identify the weight gain produced by the oxides layers generation. Weight gains associated to metallic coupons exposed to Solar_Salt_1.2%Cl and Solar_Salt_3%Cl samples were 11.4 mg/cm^2 and 38.5 mg/cm^2, respectively. These results corroborated the observation carried out in the transversal section micrographs (Fig. 9) regarding higher corrosion products amount produced over specimens tested in Solar_Salt_3%Cl sample. In addition to weight gain, descaled weight loss was analyzed over these two corrosion coupons after removing oxides layers. Then, corrosion rates as µm/year were calculated by Eq. 1 to obtain the corrosion allowances for 25 years service life time. The guide for corrosion weight loss used in the industry was adapted to A516 Gr70 properties (Table 5) to evaluate if this carbon steel was adequate for long term exposition to molten salts mixtures under evaluation within this study [40]. Corrosion rates measured over metallic specimens demonstrated again the higher aggressiveness of the molten salts mixture with greater chloride content. While corrosion rate associated to Solar_salt_1.2%Cl sample was 210 µm/year, the value obtained for Solar_salt_3%Cl sample was 535 µm/year. These results evidenced a really poor corrosion performance of A516 Gr70 carbon steel for both nitrate samples obtaining 5.25 mm and 13.38 mm corrosion allowances for Solar_salt_1.2%Cl and Solar_salt_3%Cl samples, respectively. These results represent a dramatic corrosion rate increasing regarding corrosion damage measured over metallic specimens exposed to TES-PS10 pilot plant nitrates salts during 1680 hours (9.4x and 23.9x for Solar_salt_1.2%Cl and Solar_salt_3%Cl, respectively) [29]. Finally, following the guide for corrosion weight loss used in the industry, the use of A516 Gr70 carbon steel under high chloride content solar salts was not recommended for service longer than a month.

Table 4. Corrosion damage quantitative indicators. Weight gain and corrosion rates

Molten salt sample	Chloride content (%)	Weight gain (mg/cm^2)	Corrosion rate (µm/year)
Solar_salt_1.2%Cl	1.2	11.4 ± 0.2	210 ±7
Solar_salt_3%Cl	3	38.5 ±11.4	535 ± 26

Table 5. Guide for corrosion rates used in the industry adapted to A516 Gr70 [40]

Corrosion rates range (µm/year)	**Recommendation**
> 1275	Completely destroyed within days
127 - 1274	Not recommended for service longer than a month
64 - 126	Not recommended for service longer than 1 year
14 - 63	Caution recommended, based on the specific application
0.4 - 13	Recommended for long term service

< 0.3	Recommended for long term service; no corrosion, other than as a result of surface cleaning, was evidenced

4. New materials selection analysis

Attending to previous results, the use of current materials selection focused on A516 Gr70 carbon steel is not feasible to withstand the corrosion aggressiveness increasing associated to the new nitrates salts mixtures under evaluation. However, the cost reduction potential of using non-refined nitrates salts grades would allow the specification of more expensive metallic alloys with better corrosion resistance performance. Then, the final materials selection should constitute an optimal compromise between technical and economic factors. The use of handbooks or databases is really useful to carry out a preliminary evaluation when the selection process is focused on a few properties. However, this task becomes harder when a lot of constrains such as service temperature, mechanical properties, long term stability, cost, among others, should be taken under consideration.

Ashby approach has been chosen as the method to achieve a new materials selection to be used in TES system with high chlorides content nitrate salts. This methodology is extensively used in different fields when engineers and researchers expertise should be completed with a systematic approach to solve the materials selection of complex and not well known systems [41-44]. In the present work, CES Selector software has been used to perform the proposed materials selection analysis [45, 46]. The starting point of the study was to establish the technical requirements of the metal alloy candidates. Then, constrains to take into account were as follow: (i) yield strength, (ii) tensile strength, (iii) service temperature, (iv) cost, (v) corrosion resistance, (vi) easy manufacturing, and (vii) availability.

High mechanical properties, tensile strength and yield strength, are required due to the design temperature of the TES system is in the range of 300-400 ºC cold and hot installation sides, respectively. On the one hand, metallic alloy has to work without plastification at the design conditions avoiding any permanent and non-reversible deformation. Moreover, high yield and tensile strength will also involve high maximum allowable stress (MAS) which is a critical parameter in the design of storage vessels and piping. Accordingly, high MAS would reduce the thickness of the vessels ferrules and finally the cost of the storage tanks. The minimum yield strength and tensile strength associated to A516 Gr70 carbon was fixed as mechanical constrains for the new materials selection. Attending to ASME section II standard, A516 Gr70 tensile strength range is 485-620 MPa (485 MPa was selected as minimum tensile strength required) while minimum yield strength is 260 MPa [31]. In addition to previous mechanical requirements, a minimum value for the maximum service temperature of 300 ºC was required. Fig. 15 shows, on the x-axis, the tensile strength and on the y-axis the yield strength taking into account previous mechanical and service temperature restrictions. Metals were classified in the following groups: carbon steels, cast irons, alloyed steels, stainless steels, tool steels, Ni alloys, Co alloys, and others Alloys (Cu alloys, Al alloys, Ti alloys, refractory alloys, among others).

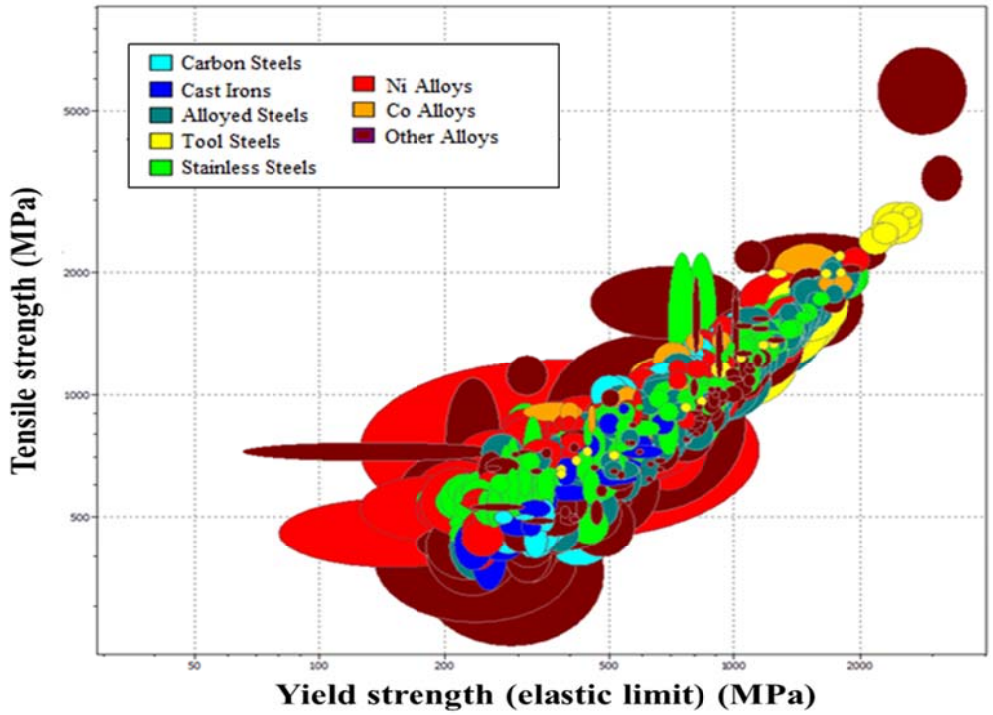

Fig. 15. Tensile strength (MPa) vs. Yield strength (MPa) for different metal alloys

Once mechanical requirements were fixed, a preliminary cost analysis was performed to discard very expensive candidates for the construction of the TES system. Then, Fig. 16 shows materials classification regarding cost per kilogram. Cast irons, carbon steels and alloyed steels are the most inexpensive materials with a cost interval in the range of 0.1-1.25 €/kg. Tool steels costs are strongly dependent on the typical alloying elements used in the manufacturing of these materials such as Cr, Mo, W, V, Ni, Co, among others. Accordingly, a very wide cost range between 2 €/kg to 20 €/kg is detected for tool steels. Stainless steels costs are placed between 0.9 €/kg for martensitic stainless steels and close to 10 €/kg for some duplex and super-austenitic stainless steels. On the other hand, Ni and Co alloys could reach costs up to 70 €/kg. Finally, "other alloys" shows a really large cost range due to families such as refractory alloys, Al alloys, Cu alloys, among others are included within this materials group. A preliminary maximum material cost of 10 €/kg was selected to discard metallic materials not feasible from economic point of view. While any Co alloys passed this economic restriction just one Ni alloy meets this requirement. Then, materials selection was limited to carbon steels, cast irons, alloyed steels, tool steels, stainless steels, one nickel alloy and some Cu-alloys included in "other materials" group (Fig. 16 b).

Cast irons are metal alloys considered brittle with a relative low thermal and mechanical shock resistance [47]. Accordingly, these characteristics discourage their use for the manufacturing of high temperature storage tanks and piping in TES systems. On the other hand, typical properties of tool steels are toughness, hardness, wear resistance and heat resistance being suitable for their use in the shaping of other materials although with negligible application in the power industry for the construction of equipment and components [48]. Then, tool steels are rejected from the materials selection for the application under evaluation. Moreover, Cu alloys are used in many industrial applications such as architecture, automotive, natural gas piping systems, seawater environments, among others [49]. However the use of these types of alloys for highly demanded applications in the range of 300-400 ºC is completely residual. Finally, the Ni-iron alloy (INVAR) was also rejected due to this candidate has the higher cost per kg within this selection. After discarding cast irons, tool steels, Cu alloys and INVAR alloy, materials selection to be

used in the TES system with high chlorides content nitrates salts was focused on three main types of steels: carbon steels, alloyed steels and stainless steels.

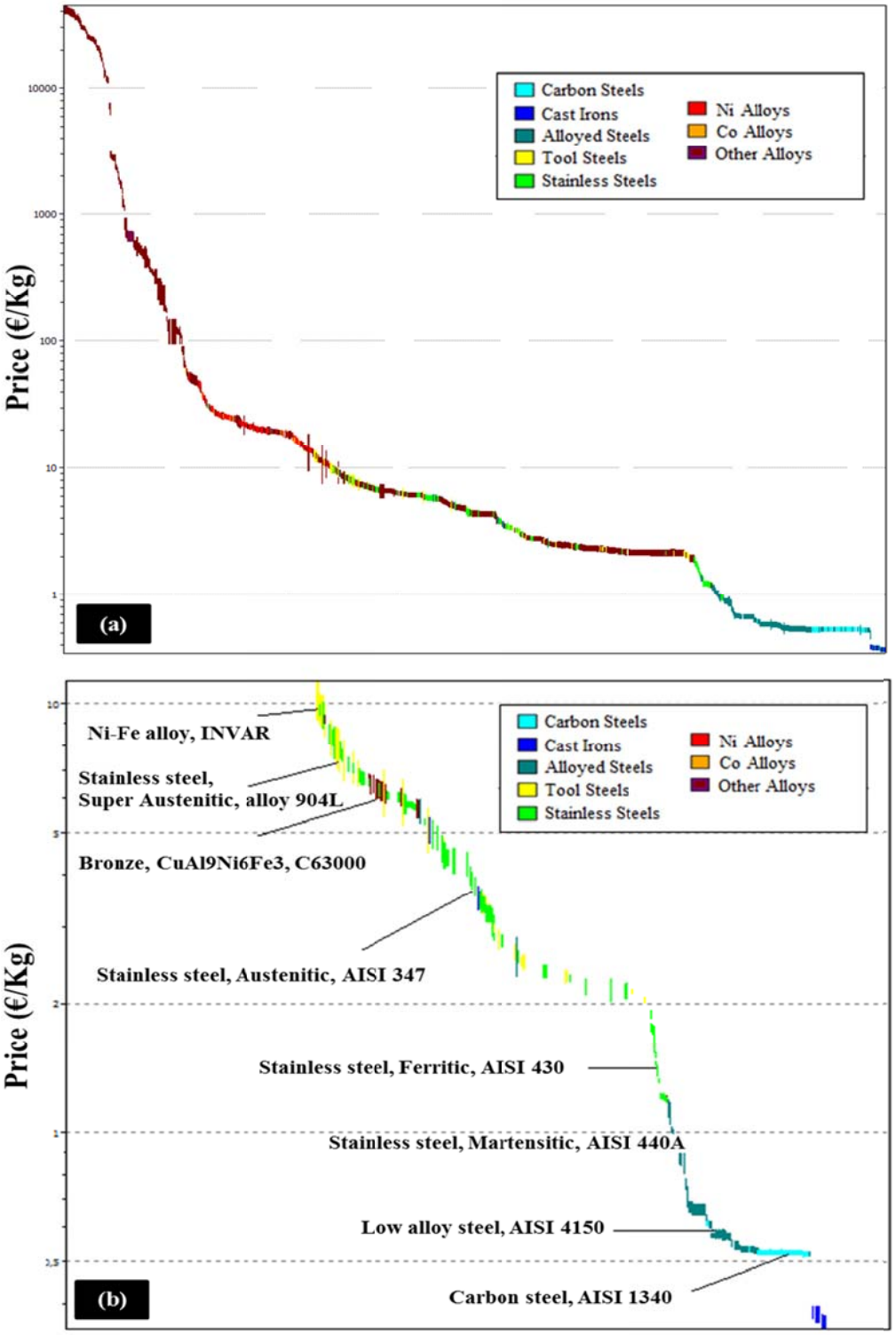

Fig. 16. Materials cost analysis: (a) Metal alloys map without cost restriction, and (b) Metal alloys map for materials up to 10 €/kg

Once mechanical requirements, service temperature range and maximum costs were fixed, corrosion resistance was also evaluated for the final selection of the candidates. CES Selector software has a qualitative database about materials durability in different environment and conditions such as organic solvents, oxidation at 500 ºC, acids, alkalis, UV radiation and water. Although corrosion performance of metal alloys in contact with nitrates salts is not included in the CES Selector software, a preliminary materials compatibility analysis was performed

evaluating the steels durability in contact with alkalis and taking into account oxidation behavior at 500 ºC. Then, Fig. 17 shows, on the x-axis, the material cost as €/kg and on the y-axis the materials durability to alkalis (Fig. 17 a) and oxidation at 500 ºC (Fig. 17 b). Materials durability information provided by CES Selector software is very qualitative classifying metal alloys as an unacceptable, limited use, acceptable or excellent. Thus, corrosion rates data are not available for a more detailed discussion. Carbon steels and alloyed steels are classified for both scenarios, alkalis exposition and oxidation at 500 ºC, as "acceptable" while stainless steels (ferritic, austenitic, martensitic and duplex) as "excellent". It is clear how the corrosion resistant improvement is directly related with cost increasing due to the presence of beneficial alloying elements such as Ni and Cr. As a general tendency, it could be assumed that Ni, Cr and Mo content increasing maximizes the corrosion resistant of metallic alloys [50, 51]. Accordingly, the formation of Ni and/or Cr oxides layers in alloyed steels and stainless steels produce a better corrosion resistance than the only formation of iron oxides in carbon steels. Moreover, the presence of Mo significantly increases the resistance to both uniform and localized corrosion [52]. Taking into account the poor corrosion performance showed by A516 Gr70 carbon steels after high-chlorides content nitrates salts exposure, carbon steels were discarded from the materials selection analysis.

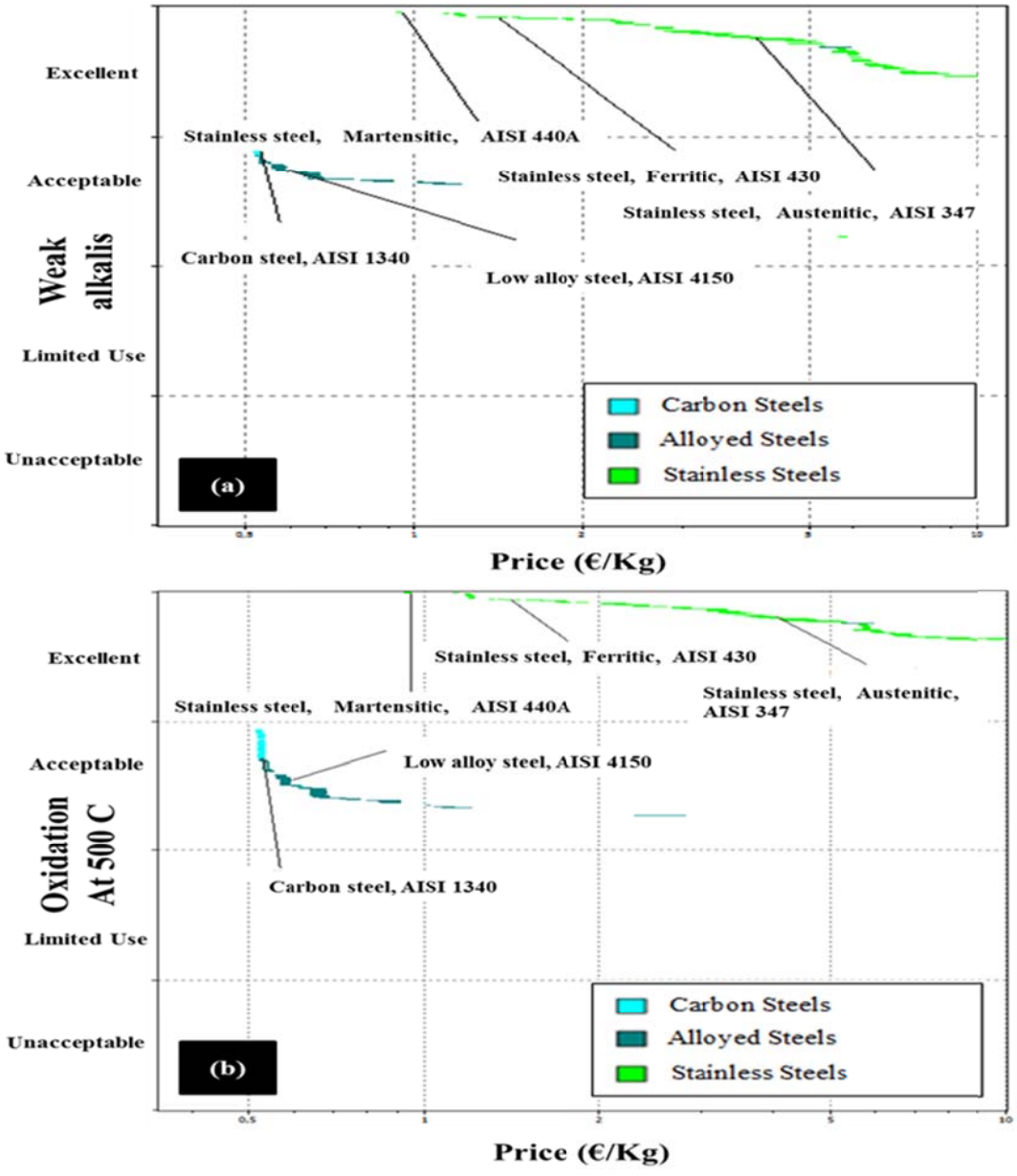

Fig. 17. Metal alloys durability: (a) Alkalis, and (b) Oxidation at 500 ºC

Once carbon steels were discarded, materials selection for this application is focused on low alloyed steels and stainless steels. Taking into account that average cost for carbon steel A516 Gr70 is close to 0.5 €/kg, the presence of expensive Ni as alloying element should be limited in the low alloyed steels and stainless steels under consideration. Then, the most interesting low alloyed steels candidates are focused on Cr-Mo alloys which are steels intended for high temperature and high pressure vessels with Cr and Mo content in the range of 0.03-9.5% and 0.35-1.10%, respectively. On the other hand, austenitic stainless steels, duplex stainless steels and precipitation hardening stainless steels were discarded for this application due to Ni content. Then, martensitic and ferritic stainless steels were selected as preliminary candidates as the most cost competitive alloys inside the stainless steels family (Cr content up to 18%). Costs associated to these new materials selection is in the range of 0.6 €/kg (low alloyed steel with the lowest content of Cr and Mo) and 1.5 €/kg (ferritic stainless steel). Corrosion tests should be executed in future tests to analyze the corrosion performance of the new candidates discussed above to obtain a technical-economical optimization of the final materials selection to be used in this application.

5. Conclusions

This study evaluates the influence of chlorides concentration in the corrosion mechanism and attack morphology of carbon steel A516 Gr70 in addition to discuss the feasibility of using solar salts mixtures with chloride content in the range of 1.2-3% by weight as storage fluid in commercial CSP projects. Thus, corrosion tests were performed during 1581 hours under N_2 cover gas to carry out a quantitative and qualitative characterization of the corrosion damage.

A516 Gr70 carbon steel visual inspection showed uniform corrosion after being exposed to Solar_Salt_1.2%Cl and Solar_Salt_3%Cl samples without detecting major localized defects. Corrosion products developed during both tests were easily broken detecting lack of adherence to base metal. Cross sections optical microscopy displayed thicker corrosion products over metallic coupons tested in the sample with a chloride content of 3% by weight detecting higher porosity and delamination of the oxides layers. Moreover, corrosion damage in the HAZ of welded coupons was higher than corrosion depth measured in the base metal. Localized phenomena such as pitting, IGC, selective leaching, among others were not found after characterizing corrosion coupons transversal sections. A more detailed evaluation performed by SEM/EDS over the surface and cross section of metallic specimens showed the delaminated morphology of corrosion products in addition to Mg, Na and K enrichment of the outermost oxides layers. Furthermore, Raman spectroscopy identified the presence of hematite in outer oxides layers while inner oxides were composed by hematite and magnetite. On the other hand, A516 Gr70 carbon steel is found to be resistant to to SCC and crevice corrosion for mixtures containing up to 3% by weight of chlorides, under the test conditions used in this study. Regarding quantitative corrosion indicators, corrosion rates calculation showed higher values for coupons exposed to Solar_Salt_3%Cl mixture corroborating the important effect of chloride content in the corrosion damage of this carbon steel. Finally, corrosion rates values obtained for A516 Gr70 indicated that this metal alloy was not suitable for a long term design.

In conclusion, this study demonstrates the important role of chlorides in the corrosion mechanism of A516 Gr70 carbon steel. Chloride content increasing promotes the formation of thicker corrosion products and affects to the adherence between oxides layers and metal base. Moreover, iron oxides layers delamination and porosity avoids the formation of a compact and well adhered diffusion barrier not allowing the passivation of metal alloy. This phenomenon produces a synergic process accelerating the corrosion damage over the carbon steel. Corrosion mechanism evidenced within this paper differs from corrosion damage observed in a previous work where solar salts with chloride content up to 0.4% are not aggressive enough to produce the generation of non-protective oxides [29].

On the other hand, solar salt mixtures with high chlorides content in the range of 1.2 to 3% by weight are not feasible for CSP applications taking into account the current materials selection. Accordingly, carbon steels used for the construction of both storage tanks, piping, among other components in parabolic trough collectors facilities are not corrosion resistant enough for 25 years service life time. Then, current materials selection should be replaced by higher corrosion resistant alloys being the Cr-Mo steels, martensitic stainless steels and ferritic stainless steels a first approach to be evaluated. Finally, in addition to corrosion tests for new metal alloys under consideration, a sensitivity study regarding extra cost produced by a more expensive materials selection and cost reduction associated to low purity nitrates salts should be performed to use these molten salts mixtures in commercial projects.

Acknowledgements

The research leading to these results has received funding from Spanish government (Fondo tecnológico IDI-20090393, ConSOLida CENIT 2008-1005). The work is partially funded by the Spanish government (ENE2011-28269-C03-02, ENE2011-22722, ENE2015-64117-C5-1-R (MINECO/FEDER), and ENE2015-64117-C5-2-R (MINECO/FEDER)). The authors would like to thank the Catalan Government for the quality accreditation given to their research group GREA (2014 SGR 123) and research group DIOPMA (2014 SGR 1543).

References

[1] Medium-term renewable energy market report, International Energy Agency (IEA), 2015

[2] Technology roadmap Solar Thermal Electricity, International Energy Agency (IEA), 2014

[3] V. Siva, S. Kaushik, K. Ranjan, S. Tyagic, State-of-the-art of solar thermal power plants: A review, Renewable and Sustainable Energy Reviews, 27 (2013) 258–273

[4] H. Zhanga, J. Baeyens, J. Degréve, Concentrated solar power plants: Review and design methodology, Renewable and Sustainable Energy Reviews, 22 (2013) 466–481

[5] A. Gil, M. Medrano, I. Martorell, A. Lázaro, P. Dolado, B. Zalba, L. Cabeza, State of the art on high temperature thermal energy storage for power generation. Part 1 - Concepts, materials and modelization, Renewable and Sustainable Energy Reviews, 14 (2010) 31-55

[6] M. Liu, N.H. Steven, S. Bell, M. Belusko, R Jacob, G. Will, W. Saman, F. Bruno, Review on concentrating solar power plants and new developments in high temperature thermal energy storage technologies, Renewable and Sustainable Energy Reviews, 53 (2016) 1411–1432

[7] L. Cabeza, E. Galindo, C. Prieto, C. Barreneche, A. Fernández, Key performance indicators in thermal energy storage: Survey and assessment, Renewable Energy, 83 (2015) 820–827

[8] S.M. Hasnain, Review on sustainable thermal energy storage technologies, part I: heat storage materials and techniques, Energy conversion and management, 39 (1998) 1127–1138

[9] D. Kearney, U. Herrmann, P. Nava, R. Mahoney, J. Pacheco, R. Cable, N. Potrovitza, D. Blake, H. Price, Assessment of a Molten Salt Heat Transfer Fluid in a Parabolic Trough Solar Field, Journal of solar energy engineering, 125 (2003) 170-176

[10] U. Herrmann, B. Kelly, H. Price, Two-tank molten salt storage for parabolic trough solar power plants, Energy, 29 (2004) 883–893

[11] L. Sena-Henderson, Advantages of using molten salts, SANDIA National Laboratories, 2006.

[12] R. Olivares, The thermal stability of molten nitrite/nitrates salt for solar thermal energy storage in different atmospheres, Solar Energy, 86 (2012) 2576-2583

[13] D. Kearney, B. Kelly, U. Herrmann, R. Cable, J. Pacheco, R. Mahoneye, H. Price, D. Blake, P. Navac, N. Potrovitza, Engineering aspects of a molten salt heat transfer fluid in a trough solar field, Energy, 29 (2004) 861–870

[14] P. Horsman, B. Conway, E. Yeager, Comprehensive Treatise of Electrochemistry, Vol 7, Plenum Press, 1983

[15] G. Lay, High Temperature Corrosion and Materials Applications, ASM International, 2007

[16] J. De Jong, G. Broers, Electrochemistry of the oxygen electrode in the KNO3-KO2 system, a comparative study, Electrochimica Acta, 22 (1977) 565-571

[17] I. Singh, S. Sultan, K. Balakrishnan, Cyclic voltammetric behaviour of platinum in dried and wet nitrates melt, Electrochimica Acta, 38 (1993) 2611-2615

[18] A. A. El Hosary, A.M. Shams El Din, A chronopotentiometric study of the stability of oxide ion in molten nitrates, Electrochimica Acta, 16 (1971) 143-149

[19] Abengoa solar website, Solana Generation Station description, (accessed 18.05.2016)

[20] H.J. Grabke, E. Reese, M. Spiegel, The effects of chlorides, hydrogen chloride, and sulfur dioxide in the oxidation of steels below deposits, Corrosion Science, 37 (1995), 1023-1043

[21] H. Goods H, R. Bradshaw, M. Prairie, J. Chavez, Corrosion of stainless steels and carbon steels in molten mixtures of industrial nitrates (SAND 94-8211), SANDIA National laboratories, 1994

[22] R.W. Bradshaw, W. M. Clift, Effect of chloride content of molten nitrate salt on corrosion of A516 carbon steel (SAND 2010-7594), SANDIA National laboratories, 2010

[23] ASM Handbook Volume 13A, Corrosion: Fundamentals, Testing, and Protection (ASM International). Corrosion by Molten Nitrates, Nitrites, and Fluorides (2003) 124-128.

[24] A.A. El Hosary, A. Baraka, A.I. Abdel-Rohman, Effects of Halides on the Corrosion of Mild Steel in Molten NaNO3-KNO3 Eutectic, British Corrosion Journal, 11 (1976) 228-230

[25] Q. Hu, Y.B. Qiu, X.P. Guo, J.Y. Huang, Crevice corrosion of Q235 carbon steels in a solution of NaHCO3 and NaCl, Corrosion Science, 52 (2010) 1205-1212

[26] M.Z Yang, M. Wilmott, J.L. Luo, Crevice corrosion behavior of A516-70 carbon steel in solutions containing inhibitors and chloride ions, Thin Solid Films, 326 (1998) 180-188

[27] H.P. Seifert, S. Ritter, The influence of ppb levels of chloride impurities on the stain-induced corrosion cracking and corrosion fatigue crack growth behavior of low-alloy steels under simulated boling water reactor conditions, Corrosion Science, 108 (2016) 148-159

[28] L. Cao, G.S. Frankel, N. Sridhar, Effect of chloride on stress corrosion cracking susceptibility of carbon steel in simulated fuel grade ethanol, Electrochimica Acta, 104 (2013) 255-266

[29] F.J. Ruiz-Cabañas, C. Prieto, R. Osuna, V. Madina, A.I. Fernández, L.F. Cabeza, Corrosion testing device for in-situ corrosion characterization in operational molten salts storage tanks: A516 Gr70 carbon steel performance under molten salts exposure, Solar Energy Materials And Solar Cells, in press

[30] C. Kramer, C. Wilson, The phase diagram of NaNO3-KNO3, Thermochimica Acta, 42 (1980) 253–264

[31] ASME Boiler and pressure vessel code. Section II a: Ferrous material specifications, ASME, 1998.

[32] ASTM E112-13. Standard Test Methods for Determining Average Grain Size, ASTM International

[33] ASTM G1-03. Standard practice for preparing, cleaning and evaluating corrosion test specimens, ASTM International

[34] ASTM G30-97. Standard Practice for Making and Using U-Bend Stress-Corrosion Test Specimens, ASTM International

[35] ASTM G58-85. Standard Practice for Preparation of Stress-Corrosion Test Specimens for Weldments, ASTM International

[36] ASTM G78-01. Standard Guide for Crevice Corrosion Testing of Iron-Base and Nickel-Base Stainless Alloys in Seawater and Other Chloride-Containing Aqueous Environments, ASTM International

[37] W. Zhao, Y. Zou, K. Matsuda, Z. Zou, Corrosion behavior of reheated CGHAZ of X80 pipeline steel in H_2S-containing environments, Materials & Design, 99 (2016) 44-56

[38] Her-Hsiung Huang, Wen-Ta Tsai, Ju-Tung Lee, Electrochemical behavior of the simulated heat-affected zone of A516 carbon steel in H_2S solution, Electrochimica Acta, 41 (1996) 1191-1199

[39] I.B. Singh, U. Sen, The effect of NaCl addition on the corrosion of mild steel in $NaNO_3$ melt, Corrosion Science, 34 (1993) 1733-1742

[40] V.S. Sastri, E. Ghali, M. Elboujdaini. Corrosion, prevention and protection. Practical solutions, John Wiley & Sons, 2007

[41] A.I. Fernandeza, M. Martínez, I. Martorell, L.F. Cabeza, Selection of materials with potential in sensible thermal energy storage, Solar Energy Materials and Solar Cells, 94 (2010), 1723-1729

[42] A. Rashedi, I. Sridhar, K.J. Tseng, Multi-objective material selection for wind turbine blade and tower: Ashby's approach, Materials & Design, 37 (2012), 521-532

[43] M. C. L. de Oliveira, G. Ett, R.A. Antunes, Materials selection for bipolar plates for polymer electrolyte membrane fuel cells using the Ashby approach, Journal of Power Sources, 206 (2012), 3-13

[44] G. P. Reddy, N. Gupta, Material selection for microelectronic heat sinks: An application of the Ashby approach, Materials & Design, 31 (2010), 113-117

[45] CES Selector 2016 Software, Granta Design Ltd, Cambridge, 2016

[46] M.F. Ashby, H. Shercliff, and D. Cebon, Materials: Engineering, Science, Processing and Design, 2nd ed., Butterworth Heinemann, Oxford, 2010, 203–224

[47] X. Wang, W. Zhang, B. Guo, W. Zhao, The characteristics of microcrack initiation process in cast iron materials under thermal shock test, Materials Science and Engineering: A, 609 (2014), 310-317

[48] G. Roberts, G. Krauss, R. Kennedy, Tool Steels, ASM International, 1998

[49] J.R. Davis, Tool Steels, Copper and copper alloys, ASM International, 2001

[50] W.A. Badawy, K.M. Ismail, A.M. Fathi, Effect of Ni content on the corrosion behavior of Cu–Ni alloys in neutral chloride solutions, Electrochimica Acta, 50 (2005), 3603-3608

[51] J.R. Hayes, J.J. Gray, A.W. Szmodis, C.A. Orme, Influence of Chromium and Molybdenum on the Corrosion of Nickel-Based Alloys, Corrosion, 62 (2006), 491-500

[52] M.I. Hazza, M.E. El-Dahshan, The effect of molybdenum on the corrosion behaviour of some steel alloys, Desalination, 95 (1994), 199-209